Sliding Mode Control-Based Autopilots for Leaderless Consensus of Unmanned Aerial Vehicles

Sachit Rao and Debasish Ghose

***Abstract*— In this brief, decentralized sliding mode controllers that enable a connected and leaderless swarm of unmanned aerial vehicles (UAVs) to reach a consensus in altitude and heading angle are presented. In addition, sliding mode control-based autopilot designs to control those states for which consensus is not required are also presented. By equipping each UAV with this combination of controllers, it can autonomously decide on being a member of the swarm or fly independently. The controllers are designed using a coupled nonlinear dynamic model, derived for the YF-22 aircraft, where the aerodynamic forces and moments are linear functions of the states and inputs.**

***Index Terms*— Autopilot, consensus, sliding mode control (SMC), swarms, unmanned aerial vehicles (UAVs).**

I. Introduction

THE ability of the members of a leaderless swarm of unmanned aerial vehicles (UAVs) to reach a consensus among themselves becomes useful when the swarm is assigned to perform search or surveillance missions. By choosing the leaderless structure, the swarm behavior is not dependent on a single member and each member of the swarm can now react independently against adverse circumstances. Applications related to the achievement of consensus in leaderless swarms of spacecraft or robotic systems can be found in [1] and other applications dependent on the group behavior of swarms with different structures are described in [2] and [3]. In this brief, decentralized sliding mode controllers (SMCs) [4] that enable the members of a swarm of UAVs to reach a consensus in altitude and heading angle are presented. In addition, an SMC-based autopilot is also designed, which when coupled with the consensus controller, allows each member to act independently.

In the literature, SMC theory has been applied to design decentralized controllers for consensus and formation control of swarms of dynamic agents. However, in most of the designs, a leader–follower framework is used and for the formation control problem, kinematic relations between the leader and followers are used to define the formation shape. Decentralized SMC designs that lead to the achievement of average consensus in a leaderless swarm of agents, modeled as single integrators, are presented in [5]. Terminal sliding mode algorithms for the achievement of finite-time consensus in a swarm of mobile robots with leaders and followers are presented in [6]. For a similar application with the added benefit of tracking a target, a decentralized formation controller using artificial potential functions and SMC is designed in [7]. In the context of UAVs, higher order sliding mode (HOSM) control-based algorithms have been developed in [8] to maintain the shape of a UAV formation. For the same problem, SMCs dependent on the inversion properties of input–output maps that determine formation flying have been designed in [9]. Concepts from nonlinear control theory have also been applied to solve the formation control problem. In [10] and [11], nonlinear dynamic inversion-based formation control laws, again in the leader–follower framework, have been presented. Both these references use the YF-22 aircraft model. Decentralized robust feedback linearizing controllers coupled with high-gain observers that allow a swarm of UAVs to track a leader UAV, again for formation flying, have been presented in [12].

An intuitive approach chosen for the design of autopilots is to decouple and/or linearize the dynamics of the longitudinal and lateral states. The implementation of well-known algorithms such as gain scheduling and its variants designed for linear parameter-varying systems can be found in [13]–[15]. Autopilots are also designed as SMCs as these lend the property of insensitivity to parameter variations to the closed-loop dynamics. In [16] and [17], SMCs are designed for the control of the lateral states using linear models. A combination of a min–max controller and an SMC is proposed to control the longitudinal states in [18] and an HOSM controller for the control of aircraft pitch is presented in [19]. The design of decoupled output tracking SMCs to control the roll angle and angle of attack (AOA) for aircraft that performs nonlinear maneuvers is presented in [20]. A combination of SMC and adaptive controllers that yield estimates of certain states for flight path control can be found in [21]. Other control approaches have also been implemented for flight control. A receding horizon control algorithm has been presented for the control of longitudinal states in [22]. A path tracking controller based on the nonlinear model predictive control technique has been proposed in [23]. An airspeed controller using the nonlinear dynamic inversion method, which considers engine dynamics, has been designed in [24].

In this brief, SMC-based autopilots and controllers that lead to consensus in altitude and heading angle, while satisfying the coordinated turn constraint, in a leaderless swarm of UAVs, are presented. Each UAV is modeled by a coupled and nonlinear six degrees-of-freedom dynamic model. For simplicity, a constant air velocity model is used. The primary motivation to use SMC theory, which yields discontinuous control inputs, for the design of these controllers is to make

Manuscript received October 10, 2012; revised March 21, 2013 and August 5, 2013; accepted November 9, 2013. Manuscript received in final form November 16, 2013. Date of publication December 13, 2013; date of current version July 24, 2014. This work was supported in part by the IISc Centenary Post-Doctoral Fellowship Program and in part by UKIERI. Recommended by Associate Editor A. Zolotas.

S. Rao is with Systemantics India Pvt Ltd., Bangalore 560078, India (e-mail: sachit@systemantics.com).

D. Ghose is with the Guidance, Control, and Decision Systems Laboratory, Department of Aerospace Engineering, Indian Institute of Science, Bangalore 560012, India (e-mail: dghose@aero.iisc.ernet.in).

Digital Object Identifier 10.1109/TCST.2013.2291784

the closed-loop dynamics insensitive to parameter variations and disturbances. Note that the chattering phenomenon that accompanies the use of discontinuous control can be avoided by the use of HOSM controllers or the implementation of its continuous approximation. In this brief, the latter technique is used. Since the UAV is a multi-input, multi-output system, the design of controllers that yield consensus in different states simultaneously, while ensuring overall stable closed-loop behavior, is a challenge. To implement the proposed SMCs, the knowledge of only those aerodynamic coefficients that relate the control inputs and the forces and moments is required. In addition, as the control is decided only by the sign of the switching function, by changing this function and the control magnitude, the controller can be used as an autopilot or for consensus, and hence the UAV can act independently or be a part of the swarm. A case demonstrating this scenario, where one UAV disconnects itself from the swarm and flies independently, is simulated. This result can be considered to be a preliminary result for the development of SMC-based consensus controllers for swarms with time-varying topologies. These properties form the motivations for the use of SMCs in the context of UAVs and form the main contributions of this brief.

The consensus controllers are developed using basic results of algebraic graph theory [25], [26]. The UAVs are considered to be the vertices of a connected and balanced graph with the edges forming the communication links through which information of only those states for which consensus is desired, for example, altitude, is transmitted. The controllers are not dependent on the kinematic structure of the swarm, and hence each of these states, and not their combination, is controlled. The swarm is assumed to be made up of the same type of UAVs. The results presented in this brief are based on the SMC-based consensus algorithms for connected swarms of dynamic agents developed in [27]. The proposed controllers are implemented for UAVs represented by the YF-22 aircraft model, as described in [10].

This brief is organized as follows. In Section II, the nonlinear dynamic model of the UAV and the role of SMCs for control and consensus are presented. In Section III, SMCs for the control of altitude, heading, and roll angles as well as those for consensus in these states are designed. This section also includes the closed-loop stability analysis. Finally, in Section IV, the simulation results of implementing the proposed control laws are presented.

II. Preliminaries

In this section, some basic results of SMC theory are first presented and these results are then used to develop a constant air velocity dynamic model. Each UAV has an aileron, an elevator, a rudder, and a throttle as its control inputs and where the aerodynamic forces and moments are affine functions of these inputs. Short notations of the type $c_\alpha = \cos\alpha, s_\alpha = \sin\alpha$, and $t_\alpha = \tan\alpha$ are used wherever necessary.

A. Role of Sliding Modes

As the SMC algorithm, [4], is well known, only a brief introduction to its application in the context of a swarm of dynamic agents is presented. In general, this algorithm, developed for control-affine dynamical systems, requires the design of functions of the system states, known as the switching surfaces, and controls, which are discontinuous on them. Consider a swarm of N dynamic agents, $N \geq 2$, where each agent is defined by the second-order dynamics $\ddot{x}_i = u_i,\ i = 1, \cdots, N,\ x_i, u_i \in \Re$, where x_i is the state and u_i is the input to the ith agent. To solve the consensus problem, the inputs u_i should be selected so that the agents' states satisfy $x_i = x_j,\ i, j = 1, \cdots, N,\ i \neq j$.

First, consider the simple case of a single agent of the swarm, for which u_i should be designed as an SMC so that $x_i \to x_d$, where, $\dot{x}_d = 0$. For this problem, by expressing the dynamics in the form $\dot{x}_{i1} = x_{i2},\ \dot{x}_{i2} = u_i$, the switching function is chosen as

$$S = x_{i2} + c\,(x_{i1} - x_d)\,,\ c > 0. \tag{1}$$

To design the control u_i, the derivative $\dot{S}$ is evaluated. Hence, from $\dot{S} = u_i + cx_{i2}$, u_i is chosen as the sum

$$\begin{aligned} u_i &= u_{i\text{eq}} + u_{i\text{disc}} \quad u_{i\text{eq}} = -cx_{i2} \\ u_{i\text{disc}} &= -M_A \text{sign}(S),\ M_A > 0 \end{aligned} \tag{2}$$

so that sliding mode occurs on $S = 0$ within a finite-time interval. As a result, the closed-loop dynamics are given by the reduced-order dynamics $\dot{x}_{i1} = -c\,(x_{i1} - x_d)$, which is known as sliding mode and is dependent only on the parameter c. This property reflects the insensitivity of sliding modes to system parameters.

In the case of consensus in a swarm, as shown in [27], the SMC-based consensus algorithms are developed by representing the swarm as an algebraic graph with N nodes. With the assumptions that this algebraic graph is connected, balanced, and has a time-invariant topology, for such a graph, denoted by G, an $N \times N$ symmetric and positive semidefinite matrix with rank $(N-1)$, known as the Laplacian matrix, $L(G)$, can be formulated. It is the property of this matrix that aids in the development of the consensus algorithms. To design the inputs u_i as SMCs so that the agents reach a consensus, the switching surface for agent i is selected as

$$S_i = \dot{x}_i + \gamma\, L(G)_i \mathbf{x},\ \mathbf{x} = [x_1 \cdots x_N]^T\,,\ \gamma > 0 \tag{3}$$

where $L(G)_i$ is the ith row of $L(G)$. Now, u_i is chosen in the form (2), but with

$$u_{i\text{eq}} = -\gamma\, L(G)_i \dot{\mathbf{x}},\ u_{i\text{disc}} = -M_C \text{sign}(S_i),\ M_C > 0 \tag{4}$$

so that sliding mode occurs on $S_i = 0$ at the finite-time instant $T_{Si} = |S_i(t=0)|/M$. As a result, the closed-loop swarm dynamics become $\dot{\mathbf{x}} = -\gamma\, L(G)\mathbf{x}$, which implies that the agents asymptotically reach the consensus value

$$x_{Cs} = \frac{1}{N}\sum_{i=1}^{N} x_i(t = T_s) \tag{5}$$

where $T_S = \max(T_{Si}),\ i = 1, \cdots, N$. It can be seen that these dynamics are also of reduced order and are dependent only on the matrix $L(G)$ and γ.

In this brief, switching surfaces are selected in the form (1) for the autopilot design and (3) for the case of consensus.

To conclude this section, the procedure that is followed to analyze the closed-loop behavior of systems controlled using SMCs is discussed using the case of controlling a single agent. From [4], this analysis is performed by calculating the equivalent controls, which are the continuous versions of those inputs that enforce sliding mode, and substituting them in the closed-loop dynamics. In the single agent case, the equivalent control is calculated as the solution to $\dot{S} = 0$ and is given by $u_{i\text{eq}}$ in (2). Now, by substituting $u_{i\text{eq}}$ in the dynamics of x_{i2}, it can be seen that $x_{i2} \to 0$ as well. These results imply that the closed-loop dynamics are asymptotically stable. This procedure is used to analyze the closed-loop dynamics of the UAV resulting from the implementation of the proposed controllers.

B. UAV Dynamics

The nonlinear UAV dynamic model presented in [10, Sec. 3.2], where the air velocity of the UAV is time varying, is used. Denoting the drag, lift, thrust, and side forces as D, L, T, and Y, respectively, and m_P as the pitching moment, the dynamics of the airspeed V_a, the angle-of-attack (AOA) α, the pitch angle θ, and the pitch rate Q are

$$\begin{aligned} m\dot{V}_a &= Ys_\beta - Dc_\beta - mgs_\gamma + Tc_\beta c_\alpha && \text{(6a)}\\ mV_a c_\beta \dot{\alpha} &= -L - Ts_\alpha + mV_a\left(Qc_\beta - P_s s_\beta\right) \\ &\quad + mg\left(c_\theta c_\phi c_\alpha + s_\theta s_\alpha\right) && \text{(6b)}\\ \dot{\theta} &= Qc_\phi - Rs_\phi && \text{(6c)}\\ J_y\dot{Q} &= \left(J_z - J_x\right)PR - J_{xz}\left(P^2 - R^2\right) + \bar{c}\mathrm{m}_P && \text{(6d)}\\ s_\gamma &= c_\alpha c_\beta s_\theta - s_\beta s_\phi c_\theta - s_\alpha c_\beta c_\phi c_\theta && \text{(6e)}\\ P_s &= Pc_\alpha + Rc_\alpha,\ R_s = Rc_\alpha - Ps_\alpha \end{aligned}$$

where the mass m, the mean aerodynamic chord $\bar{c}$, the moments-of-inertia, about the corresponding axes, J_x, J_y, J_z, and J_{xz} are the UAV parameters, β is the side-slip angle, P and R are the roll and yaw rates, respectively, ϕ is the roll angle, and ψ is the yaw angle. Denoting the lateral aerodynamic moments as l and n, the dynamics of β, ϕ, ψ, P, and R are given by

$$\begin{aligned} mV_a\dot{\beta} &= Ds_\beta + Yc_\beta - Tc_\alpha s_\beta \\ &\quad + mg\left(s_\theta c_\alpha s_\beta + c_\theta s_\phi c_\beta - c_\theta c_\phi s_\alpha s_\beta\right) - mV_a R_s && \text{(7a)}\\ \dot{\phi} &= P + t_\theta\left(Qs_\phi + Rc_\phi\right) && \text{(7b)}\\ c_\theta\dot{\psi} &= Qs_\phi + Rc_\phi && \text{(7c)}\\ \Gamma\dot{P} &= J_{xz}\left(J_x - J_y + J_z\right)PQ - \left(J_z^2 - J_yJ_z + J_{xz}^2\right)QR \\ &\quad + b\left(J_z l + J_{xz}n\right) && \text{(7d)}\\ \Gamma\dot{R} &= \left(J_x^2 - J_xJ_y + J_{xz}^2\right)PQ - J_{xz}\left(J_x - J_y + J_z\right)QR \\ &\quad + b\left(J_{xz}l + J_xn\right),\ \Gamma = J_xJ_z - J_{xz}^2 && \text{(7e)} \end{aligned}$$

where b is the wingspan.

Denoting the aileron, elevator, and rudder deflections, which are the control inputs, by δ_a, δ_e, and δ_r, respectively, the drag force, lift force, and the pitching moment are given by

$$\mu K = C_{K0} + C_{K\alpha}\alpha + C_{KQ}\bar{c}_{Va}Q + C_{K\delta_e}\delta_e,\ K = D, L, \mathrm{m}_P \quad \text{(8a)}$$

where

$$\bar{c}_{Va} = \frac{\bar{c}}{2V_a},\ \frac{1}{\mu} = \frac{1}{2}\rho S_w V_a^2 \quad \text{(8b)}$$

where S_w is the wing area and ρ is the air density, which is assumed to be a constant. The moments l, n, and the side force Y are of the form

$$\begin{aligned} \mu K &= C_{K0} + C_{K\beta}\beta + \bar{b}\left(C_{KP}P + C_{KR}R\right) + C_{K\delta_a}\delta_a \\ &\quad + C_{K\delta_r}\delta_r \\ K &= l, n, Y,\ \bar{b} = \frac{b}{2V_a}. \end{aligned} \quad \text{(9)}$$

With the expressions for the moments l and n, the constants

$$\Gamma C_{PK} = \left(J_z C_{lK} + J_{xz}C_{nK}\right) \quad \text{(10a)}$$

$$\Gamma C_{RK} = \left(J_{xz}C_{lK} + J_x C_{nK}\right),\ K = 0, \beta, P, R, \delta_a, \delta_r \quad \text{(10b)}$$

are defined to denote the coefficients that relate the aileron and rudder inputs to the dynamics of P and R, respectively. These equations differ from those presented in [10] in the use of some notations, for example, the use of D in place of C_D, and so on, and the equations of the dynamics of P, Q, and R, which are used here in an expanded form. In addition, more details on the physical significance of these expressions can be found in [10].

It can be seen from (8), that the components D, L, and m_P - which primarily affect the states α and Q - are dependent only on these states. Similarly, l, n, and Y in (9), which decide the dynamics of the lateral states, are linearly dependent only on these states. These are the standard assumptions that enable the decoupled design of the UAV inputs as controls for the longitudinal and lateral states [28]. However, as will be shown in the following, the side force Y couples the dynamics of these states and this coupling is retained while designing the SMC-based autopilots and consensus controllers.

C. Constant Air Velocity Model

To derive the constant air velocity model of the UAV, the thrust force T and hence the throttle input, denoted by δ_t, that satisfies $\dot{V}_a = 0$ for a constant velocity V_{aC}, is calculated from (6a). Next, since T affects only the states α and β, this calculated value is substituted in these dynamics to yield the constant air velocity model. This procedure results in the dynamics

$$\begin{aligned} mV_{aC}c_\beta\dot{\alpha} &= -\left(L + Dt_\alpha\right) + Yt_\alpha t_\beta + mV_{aC}\left(Qc_\beta - P_s s_\beta\right) \\ &\quad + \frac{mgc_\theta}{c_\alpha c_\beta}\left(c_\beta c_\phi + s_\alpha s_\beta s_\phi\right) && \text{(11a)}\\ mV_{aC}c_\beta\dot{\beta} &= Y + mgc_\theta s_\phi - mc_\beta V_{aC}R_s. && \text{(11b)} \end{aligned}$$

These dynamics and those of the other UAV states, which remain unchanged from (6) and (7), are used to design the SMCs. Note that since the dynamics relating δ_t and V_a is

a relative degree 1 system, δ_t can also be designed as an SMC to enforce sliding mode on a surface of the form $S_V = V_a - V_{aC} = 0$, where, V_{aC} is the desired constant airspeed. Now, it can be shown that by calculating the equivalent throttle input according to the procedure described in Section II-A, the dynamics of α and β are given by (11).

To complete the description of the UAV dynamics, the navigation equations are defined in the following equations. The altitude dynamics are given by

$$\dot{h} = V_{aC} s_\gamma \tag{12}$$

where s_γ is given by (6e). The speed of the UAV in the north and east directions (about some coordinate frame), in steady flight, that is, when $\alpha = \theta$ and $\phi = 0$, are given by

$$\dot{p}_n = V_{aC} \cos(\psi + \beta), \quad \dot{p}_e = V_{aC} \sin(\psi + \beta). \tag{13}$$

Thus, from these equations, it is clear that the heading angle, denoted by χ, is given by the sum $\chi = \psi + \beta$.

These equations are used to design the control inputs $\delta_j,\ j = a, e, r$, as SMCs for consensus in altitude and heading angle as well as for the design of autopilots for these states. In addition, in both cases, the roll angle is controlled using the coordinated turn constraint [28]

$$\phi = \dot{\chi} \frac{V_a}{g c_\theta}. \tag{14}$$

III. UAV Controllers

The controllers that enable a connected swarm of UAVs to reach a consensus and the autopilots that allow a single UAV to fly independently are designed. For the case of consensus, each UAV is assumed to have the knowledge of those states of the UAVs to which it is connected and for which consensus is desired. For example, to achieve consensus in altitude, each UAV is assumed to know the altitudes of all the UAVs to which it is connected. To design the autopilots, for simplicity, the desired state values are assumed to be a constant. Thus, if the desired altitude is, say, h_{des}, then $\dot{h}_{\text{des}} = 0$. Since the designs for the autopilot and consensus cases are almost similar, they are presented in parallel, but their individual differences are also highlighted.

A. Altitude Control

For the autopilot, the altitude h is controlled using the pitch angle θ as an intermediate control input, denoted by θ_{des}, in the form

$$\theta_{\text{des}} = \alpha - \frac{\lambda_h (h - h_{\text{des}})}{V_{aC} c_\beta} \tag{15}$$

where the constants $\lambda_h > 0$ and h_{des} is the desired altitude. Next, θ is controlled using the elevator, δ_e, which appears in the dynamics of the pitch rate Q so that $\theta \to \theta_{\text{des}}$, by enforcing sliding mode on the surface

$$S_h = Q + \lambda_{hs} (\theta - \theta_{\text{des}}) = 0, \ \lambda_{hs} > 0. \tag{16}$$

Note that since θ_{des} depends on α and β, it is not necessary that the condition $\dot{\theta}_{\text{des}} = 0$ holds.

The motivations to choose θ_{des} in the form (15) and S_h as the switching surface are as follows. It is emphasized that the following comments are provided only to obtain an intuitive understanding of these choices. Under the conditions that θ and α are small, the roll angle $\phi = 0$, and $|\beta| \neq \pi/2$, which hold for most types of aircraft in level flight, the altitude dynamics (12) simplifies to

$$\dot{h} = V_{aC} (\theta - \alpha) c_\beta. \tag{17}$$

Thus, if $\theta \to \theta_{\text{des}}$, then it is clear that $h \to h_{\text{des}}$ asymptotically at a rate decided by λ_h. In addition, with $\phi = 0$, the open-loop dynamics of θ, given by (6c), simplifies to $\dot{\theta} = Q$. Thus, S_h becomes $S_h = \dot{\theta} + \lambda_{hs} (\theta - \theta_{\text{des}}) = 0$. In turn, with the occurrence of sliding mode on $S_h = 0$, $\theta \to \theta_{\text{des}}$ asymptotically at a rate decided by λ_{hs}. It will be proved in this section on closed-loop stability analysis that the conditions $\phi = 0$ and $\dot{\alpha}, \dot{\beta} = 0$ with $|\beta| \neq \pi/2$ and bounded $\alpha > 0$ will hold with the implementation of the proposed controllers. Note that the assumption of θ and α being small, i.e., level flight at small AOA values, is also a standard one made while designing controllers for aircraft. Based on these comments, in the case of consensus, the intermediate control of the ith UAV is selected as

$$\theta_{i\text{des}} = \alpha_i - \frac{\lambda_h L_{Gi} \mathbf{h}}{V_{aC} c_{\beta i}}, \ \mathbf{h} = [h_1 \cdots h_N]^T \tag{18}$$

while the switching surface is of the form (16). In this case, the closed-loop altitude dynamics of the swarm becomes $\dot{\mathbf{h}} = -\lambda_h L_G \mathbf{h}$, which implies, based on the results of Section II-A, that the UAVs reach a consensus in altitude.

Now, based on the procedure described in Section II-A, δ_e is selected by first evaluating $\dot{S}_h$. Hence, from

$$\dot{S}_h = \dot{Q} + \lambda_{hs} \left[\dot{\theta} - \dot{\theta}_{\text{des}}\right] = \frac{K_e}{\mu} \delta_e + F_h \tag{19a}$$

where

$$K_e = \frac{\bar{c}}{J_y} C_{\text{m}\delta_e} + \frac{\lambda_{hs}}{m V_{aC} c_\beta} \left(C_{L\delta_e} + C_{D\delta_e} t_\alpha\right) \tag{19b}$$

and F_h consists of the terms evaluated using the open-loop dynamics (6c), (6d), and (11). As a result, the elevator input δ_e is chosen as

$$\delta_e = -\left[F_h + M_h \text{sign}(S_h)\right] \frac{\mu}{K_e} \tag{20}$$

with $M_h > 0$ so that sliding mode occurs on $S_h = 0$. Note that the paramter λ_{hs} should be chosen so that $K_e \neq 0$. The convergence of $\theta \to \theta_{\text{des}}$ as well as $h \to h_{\text{des}}$ with the implementation of these controllers is shown in the closed-loop stability analysis, presented in Section III-C. This analysis is performed by calculating the equivalent elevator input, denoted by $\delta_{e\text{eq}}$, as the solution to $\dot{s}_h = 0$ and substituting it in the dynamics of the other states. In the case of consensus, if the closed-loop system is stable, then $h_i \to h_C,\ i = 1, \cdots, N$, where, h_C is the constant consensus value, which has a form similar to (5).

B. Control of Heading and Roll Angles

In this section, the aileron, δ_a, and the rudder, δ_r, are designed to control the heading and roll angles.

1) Control of χ: From the expressions for the heading angle $\chi = \psi + \beta$, the side force Y, given by (9), and the dynamics of β, given by (11b), it can be observed that the dynamics between χ and the controls $\delta_{a,r}$ is a relative degree 1 system. Hence, in the autopilot case, given χ_{des} as the desired heading angle, χ can be controlled by enforcing sliding mode on a surface of the form $S_\chi = \chi - \chi_{\text{des}} = 0$. However, this choice of control can lead to the heading angle being subjected to the chattering phenomenon. To avoid the occurrence of this behavior and make $\dot{\chi}$ and χ continuous, the switching surface to control χ for the autopilot case is chosen as

$$S_\chi = R\frac{c_\phi}{c_\theta} + \lambda_\chi\left(\chi - \chi_{\text{des}}\right),\ \lambda_\chi > 0. \tag{21}$$

In the case of consensus, the switching surface for the ith UAV is chosen as

$$S_{\chi i} = R_i\frac{c_{\phi i}}{c_{\theta i}} + \lambda_\chi L_{Gi}X,\ X = [\chi_1 \cdots \chi_N]^T. \tag{22}$$

To understand the choice of these surfaces, consider the open-loop dynamics of χ based on that of ψ, given by (7c), when the conditions $Q, \dot{\beta} = 0$ hold. Now, $\dot{\chi} = Rc_\phi/c_\theta$, and hence S_χ reduces to $S_\chi = \dot{\chi} + \lambda_\chi\left(\chi - \chi_{\text{des}}\right)$. Therefore, if sliding mode occurs on $S_\chi = 0$, then it is evident that $\chi \to \chi_{\text{des}}$ asymptotically at a rate decided by λ_χ. Similarly, in the case of consensus, the UAVs reach a consensus in heading angle whose value is similar to (5).

2) Control of ϕ: The switching surface to control the roll angle in the case of the autopilot is selected as

$$S_\phi = P + \lambda_\phi\phi + \kappa\left(\chi - \chi_{\text{des}}\right),\ \kappa = \lambda_\phi\lambda_\chi\frac{V_{aC}}{gc_\theta}\left(1 - \frac{\lambda_\chi}{\lambda_\phi}\right) \tag{23}$$

where the constant $\lambda_\phi > 0$ is chosen to be large and λ_χ is as defined in (21). The choice of this switching surface can be understood as follows. First, the coordinated turn constraint (14) is modified by replacing $\dot{\chi}$ with the expression $-\lambda_\chi\left(\chi - \chi_{\text{des}}\right)$. Next, by observing that under the conditions of $Q, R = 0$, the open-loop dynamics of ϕ, as given by (7b), reduces to $\dot{\phi} = P$. Thus, if sliding mode occurs on $S_\phi = 0$, then ϕ is governed by the first-order dynamics

$$\dot{\phi} = -\lambda_\phi\left[\phi + \lambda_\chi\frac{V_{aC}}{gc_\theta}\left(1 - \frac{\lambda_\chi}{\lambda_\phi}\right)\left(\chi - \chi_{\text{des}}\right)\right]. \tag{24}$$

Now, for a large λ_ϕ, it is evident that ϕ satisfies the modified turn constraint, which in turn implies that $\phi \to 0$ as $\chi \to \chi_{\text{des}}$. Analogous to the case of the autopilot, for the case of consensus, the switching surface for the ith UAV is chosen as

$$S_{\phi i} = P_i + \lambda_\phi\phi_i + K_iX,\ K_i = \lambda_\phi\lambda_\chi\frac{V_{aC}}{gc_{\theta i}}L_{Gi}\left(\mathbf{I} - \frac{\lambda_\chi}{\lambda_\phi}L_G\right). \tag{25}$$

In this case, $\phi_i \to 0$ as $L_{Gi}X \to 0$.

3) Design of δ_a and δ_r: The control inputs δ_a and δ_r are now selected to enforce sliding mode on the surfaces S_χ and S_ϕ (similarly, $S_{\chi i}$ and $S_{\phi i}$ for the case of consensus). Thus, differentiating S_χ, S_ϕ leads to

$$\begin{bmatrix}\dot{S}_\chi\\ \dot{S}_\phi\end{bmatrix} = \mathbf{D}\begin{bmatrix}\delta_a\\ \delta_r\end{bmatrix} + \begin{bmatrix}F_\chi\\ F_\phi\end{bmatrix}$$
$$\mathbf{D} = \frac{1}{\mu}\times\begin{bmatrix}\left(\frac{bc_\phi}{c_\theta}C_{R\delta_a} + \frac{\lambda_\chi}{mV_{aC}c_\beta}C_{Y\delta_a}\right) & \left(\frac{bc_\phi}{c_\theta}C_{R\delta_r} + \frac{\lambda_\chi}{mV_{aC}c_\beta}C_{Y\delta_r}\right)\\ \left(bC_{P\delta_a} + \frac{\kappa}{mV_{aC}c_\beta}C_{Y\delta_a}\right) & \left(bC_{P\delta_r} + \frac{\kappa}{mV_{aC}c_\beta}C_{Y\delta_r}\right)\end{bmatrix} \tag{26}$$

where F_χ and F_ϕ are the terms evaluated using the open-loop dynamics. Therefore, by choosing

$$\begin{bmatrix}\delta_a\\ \delta_r\end{bmatrix} = -\mathbf{D}^{-1}\begin{bmatrix}F_\chi + M_\chi\,\text{sign}(S_\chi)\\ F_\phi + M_\phi\,\text{sign}(S_\phi)\end{bmatrix},\ M_\chi, M_\phi > 0 \tag{27}$$

sliding mode occurs on $S_\chi = 0$ and $S_\phi = 0$ within a finite-time interval. Note that during normal flying conditions, that is, when $\left|\beta, \phi, \theta\right| < \pi/2$, all the trigonometric terms that appear in $\mathbf{D}$ are positive. In addition, since the matrix $\mathbf{D}$ has to be nonsingular, the parameters λ_χ and λ_ϕ are chosen appropriately. For the case of consensus, the aileron and rudder inputs of the ith UAV are calculated similarly, but now using the Laplacian matrix L_G. The closed-loop dynamics, which result with the occurrence of sliding mode on $S_\chi = 0$ and $S_\phi = 0$, are analyzed in the following section.

C. Closed-Loop Stability

To validate the proposed controller designs, the closed-loop UAV dynamics are now analyzed by linearzing them about the desired equilibrium points. It will be shown that if the UAV parameters satisfy a few conditions, then these equilibrium points are indeed asymptotically stable. The case of autopilots is first considered. Note that the closed-loop dynamics are of reduced order because, with the occurrence of sliding mode on $S_h = 0$, $S_\chi = 0$, and $S_\phi = 0$, the relations

$$\begin{aligned}Q &= -\lambda_{hs}\left(\theta - \alpha + \frac{\lambda_h\left(h - h_{\text{des}}\right)}{V_{aC}c_\beta}\right)\\ P &= -\lambda_\phi\phi - \kappa\left(\chi - \chi_{\text{des}}\right)\\ R &= -\frac{c_\theta}{c_\phi}\lambda_\chi\left(\chi - \chi_{\text{des}}\right)\end{aligned} \tag{28}$$

respectively, hold and hence there is no need to analyze the dynamics of these states.

To perform the analysis, following the procedure described in Section II-A, the equivalent controls should be calculated. However, the closed-loop dynamics of h, θ, ϕ, and ψ, linearized about $\hat{\theta} = \hat{\alpha} = \alpha_0 > 0, \hat{\phi}, \hat{\beta} = 0$, and

given by

$$\dot{\hat{h}} = V_{aC}\left(\hat{\theta} - \hat{\alpha}\right)$$

$$\dot{\hat{\theta}} = -\lambda_{hs}\left(\hat{\theta} - \hat{\alpha} + \frac{\lambda_h\left(\hat{h} - h_{\text{des}}\right)}{V_{aC}}\right)$$

$$\dot{\hat{\psi}} = -\lambda_\chi\left(\hat{\psi} + \hat{\beta} - \chi_{\text{des}}\right) \tag{29a}$$

$$\dot{\hat{\phi}} = -\lambda_\phi\hat{\phi} - \left(\kappa + \lambda_\chi s_{\alpha_0}\right)\left(\hat{\psi} + \hat{\beta} - \chi_{\text{des}}\right)$$

$$s_{\alpha_0} = \sin\alpha_0 \tag{29b}$$

can be analyzed without calculating these inputs explicitly. It can be seen from (29) that by choosing the switching surface parameters $\lambda_{hs}, \lambda_h, \lambda_\chi$, and λ_ϕ appropriately, $\hat{\theta} \to \hat{\alpha}$, and hence $\hat{h} \to h_{\text{des}}$. In addition, as $\hat{\psi} \to \left(\chi_{\text{des}} - \hat{\beta}\right)$, the state $\hat{\phi} \to 0$ independently of $\hat{\theta}$. These results and (28) also imply that the equilibrium points of the states P, Q, and R, denoted by $\hat{P}$, $\hat{Q}$, and $\hat{R}$, respectively, satisfy $\hat{P} = \hat{Q} = \hat{R} = 0$.

Note that it is now sufficient to analyze only the closed-loop dynamics of $\hat{\alpha}, \hat{\beta}$ using these results and for which, the equivalent controls $\delta_{j\text{eq}}$, $j = e, a, r$ are calculated as the solutions to $\dot{S}_h = \dot{S}_\chi = \dot{S}_\phi = 0$. For this analysis, the linearized versions of these controls, denoted by $\hat{\delta}_{j\text{eq}}$, $j = e, a, r$, are calculated. Observing that in the vicinity of the equilibrium values, the relations $\dot{S}_h, \dot{S}_\chi, \dot{S}_\phi = 0$, reduce to $\dot{\hat{Q}} = \dot{\hat{R}} = \dot{\hat{P}} = 0$, respectively, from (8), (9), and (10), these equivalent controls assume the form

$$\hat{\delta}_{e\text{eq}} = -\frac{C_{\text{m}_P\alpha}}{C_{\text{m}_P\delta_e}}\hat{\alpha}$$

$$\begin{bmatrix}\hat{\delta}_{a\text{eq}}\\ \hat{\delta}_{r\text{eq}}\end{bmatrix} = \frac{1}{C_{P\delta_a}C_{R\delta_r} - C_{P\delta_r}C_{R\delta_a}}\begin{bmatrix}\left(C_{P\delta_r}C_{R\beta} - C_{R\delta_r}C_{P\beta}\right)\\ \left(C_{R\delta_a}C_{P\beta} - C_{P\delta_a}C_{R\beta}\right)\end{bmatrix}\hat{\beta}. \tag{30}$$

It can now be shown, using (30), that the linearized dynamics of $\hat{\alpha}, \hat{\beta}$ become

$$\dot{\hat{\alpha}} = \frac{1}{\mu m V_{aC}}A_\alpha\left(\hat{\alpha} - \alpha_0\right) + \frac{g t_{\alpha_0}}{V_{aC}}\left(\hat{\alpha} - \hat{\theta}\right) + \frac{\partial\dot{\alpha}}{\partial\beta}\hat{\beta}$$

$$t_{\alpha_0} = \tan\alpha_0 \tag{31a}$$

$$\dot{\hat{\beta}} = \frac{1}{\mu m V_{aC}}A_\beta\hat{\beta} \tag{31b}$$

where

$$A_\alpha = \left[\left(C_{D0} + C_{D\alpha}\alpha_0 - \frac{C_{\text{m}_P\alpha}}{C_{\text{m}_P\delta_e}}\alpha_0\right)\frac{1}{\cos^2\alpha_0} + \left(C_{L\alpha} + C_{D\alpha}t_{\alpha_0}\right) - \frac{C_{\text{m}_P\alpha}}{C_{\text{m}_P\delta_e}}\left(C_{L\delta_e} + C_{D\delta_e}t_{\alpha_0}\right)\right] \tag{31c}$$

$$A_\beta = C_{Y\beta} + \frac{1}{C_{P\delta_a}C_{R\delta_r} - C_{P\delta_r}C_{R\delta_a}}\left[C_{Y\delta_a}\ C_{Y\delta_r}\right] \times \begin{bmatrix}\left(C_{P\delta_r}C_{R\beta} - C_{R\delta_r}C_{P\beta}\right)\\ \left(C_{R\delta_a}C_{P\beta} - C_{P\delta_a}C_{R\beta}\right)\end{bmatrix} \tag{31d}$$

and the term $\partial\dot{\alpha}/\partial\beta$ is calculated from (11a). As is evident from these dynamics, if $A_\beta < 0$, then $\hat{\beta} \to 0$ independently of any other state. As a result and since it has been shown that $\hat{\theta} \to \hat{\alpha}$, the closed-loop dynamics of $\hat{\alpha}$ is also asymptotically stable only if the constant $A_\alpha < 0$. In the case of the UAV model selected in this brief, the UAV parameters satisfy these relations, and hence the closed-loop UAV dynamics are stable. Note that these requirements arise naturally with the chosen UAV model as it can be considered to be an under-actuated system. For example, it is only the elevator, which is available to control both the altitude and the AOA. This result is also supported by the simulation results. The stability results for the case of consensus are the same. The differences lie only in the steady-state values of h_i and χ_i, as now, these values are constants and are of the form (5).

TABLE I
YF-22 PARAMETERS

Airspeed, AOA, Altitude	$V_a = 42$ m/s, $\alpha = 3^\circ$, $h = 120$ m
Mean chord, Wingspan, Mass	$\bar{c} = 0.76$ m, $b = 1.96$ m, $m = 20.64$ kg
Inertial parameters	$J_x = 1.61$, $J_y = 7.51$, $J_z = 7.18$, $J_{xz} = -0.59$, in kg m^2
Longitudinal Aerodynamic Coefficients	$C_{L\delta_e} = 0.19$, $C_{D\delta_e} = -0.034$, $C_{\text{m}\delta_e} = -0.36$
Longitudinal Aerodynamic Coefficients	$C_{Y\delta_a} = 0.18$, $C_{l\delta_a} = -0.06$, $C_{n\delta_a} = -0.04$ $C_{Y\delta_r} = -.46$, $C_{l\delta_r} = 0.014$, $C_{n\delta_r} = -0.06$
Control Deflection Bounds	$\lvert\delta_e\rvert \le 8^\circ$, $\lvert\delta_a\rvert \le 8^\circ$, $\lvert\delta_r\rvert \le 8^\circ$

In the following section, the simulation results of implementing the proposed autopilot and decentralized consensus controllers on connected swarms of UAVs with time-invariant and simple time-variant topologies are presented.

IV. Implementation and Simulation Results

The proposed autopilot designs are implemented on the YF-22 research aircraft model described in [10]. In Table I, relevant parameters of this aircraft, derived at the mentioned trim conditions, are listed. For $\alpha \in [0.5^\circ, 20^\circ]$, $\beta \in [-25^\circ, 25^\circ]$, $V_a \in [40, 60]$ m/s, and the switching surface parameters $\lambda_{hs}, \lambda_\phi, \lambda_\chi > 0$ with $\lambda_\phi > \lambda_\chi$, it can be shown that these parameters satisfy the requirements of $K_e \neq 0$ in (19b), $|\mathbf{D}| \neq 0$ in (27), and $A_\alpha, A_\beta < 0$ in (31).

The simulations for consensus in altitude and heading angle are performed for swarms with time-invariant and time-variant topologies. In the latter case, one UAV breaks away from the swarm at some time instant $t = T_C > 0$ and engages its autopilots for the control of altitude and heading angle. The graphs of these swarms are shown in Fig. 1(a) and (b) and their corresponding Laplacian matrices are given by

$$L_I = \begin{bmatrix}2 & -1 & -1\\ -1 & 2 & -1\\ -1 & -1 & 2\end{bmatrix},\ L_V = \begin{bmatrix}1 & -1 & 0\\ -1 & 1 & 0\\ 0 & 0 & 0\end{bmatrix} \tag{32}$$

respectively. Note that for the latter case, the graph Laplacian matrix is given by L_I for $t < T_C$, and for $t \ge T_C$, its Laplacian matrix is given by L_V. A simplified block diagram that illustrates the implementation of the proposed controllers on any UAV is shown in Fig. 1. As mentioned before, for the case of consensus, only altitude and/or heading angle data need be transmitted between connected UAVs.

For both cases of simulations and for each UAV, $V_{aC} = 45$ m/s and the initial conditions, denoted using the subscript 0, are selected as $\psi_0 \in [0^\circ, 180^\circ]$, $\phi_0 \in [0^\circ, 30^\circ]$, $\alpha_0, \theta_0, \beta_0 \in [0^\circ, 5^\circ]$, $h_0 \in [140, 160]$ m, and $P_0, Q_0, R_0 = 0$.

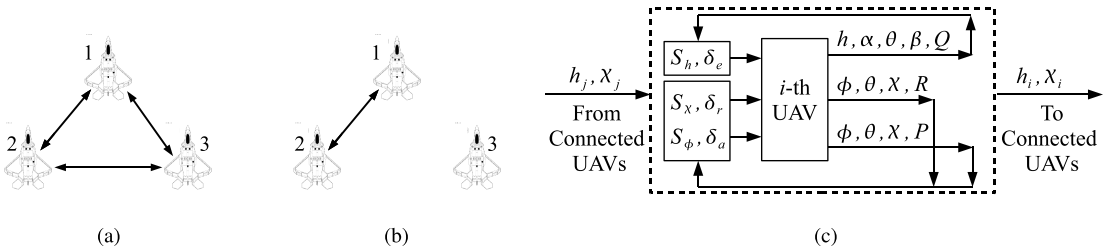

Fig. 1. Graphs of a swarm with (a) time-Invariant and (b) time-varying topologies. (c) Control block diagram.

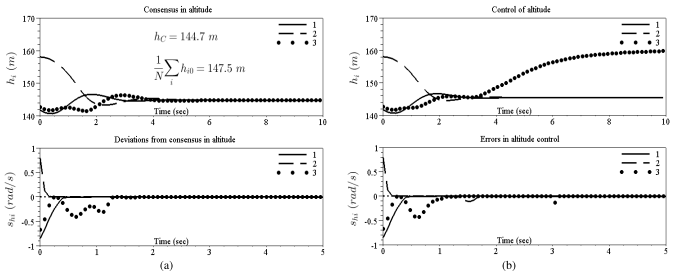

Fig. 2. Control of altitude and errors in control. (a) Time-invariant topology. (b) Time-varying topology.

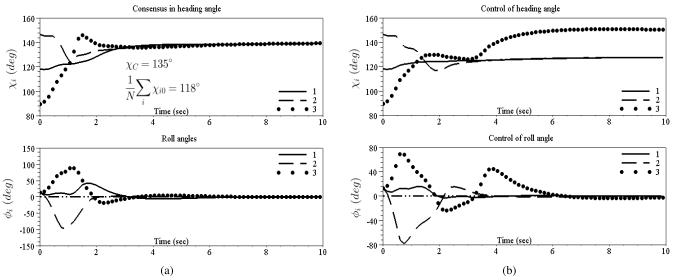

Fig. 3. Control of roll and heading angles. (a) Time-invariant topology. (b) Time-varying topology.

The single-step forward-Euler scheme with a stepsize of 1 ms is chosen as the numerical solver. This value for the stepsize was chosen to reflect a worst case scenario in implementing the SMCs. From [4], due to a discrete implementation using a stepsize, say Δ, the deviation from ideal sliding mode will also be of order Δ. The discontinuous component of each of the control inputs is replaced by its continuous approximation $u_{\text{ca}} = -(M/\varepsilon)S$ if $|S| \leq \varepsilon$, else by $u_{\text{ca}} = -M\text{sign}(S)$, where $\varepsilon = 0.01$. Though the use of this approximation results in reduced chattering [4], it also leads to the deviation from ideal sliding mode to be of order ε.

To illustrate the property of insensitivity of sliding modes to parameter variations and disturbances, for the case of the time-varying topology, the controls are computed without the equivalent control part, for example, from (20), δ_e is computed by setting $F_h = 0$. Similarly, from (27), δ_a and δ_r are calculated with $F_\chi, F_\phi = 0$. Note that with this change and from the basics of SMC theory, the magnitudes of the discontinuous control components are increased. This simulation scenario is sufficient to illustrate insensitivity as any external disturbances that act on the UAV would appear in the expression of F_h, F_χ, and F_ϕ. For the time-invariant topology case, the controllers are computed as described in the corresponding sections. As the results show, the SMCs are able to enforce sliding mode on the corresponding switching surfaces in both cases.

The achievement of consensus in altitude and the errors in the control of these states, for both cases of swarm topologies and control computations, can be observed in Fig. 2. In the time-invariant case, the UAVs reach a consensus value, given by (5), which differs from the average of their respective initial states. This difference, which is because of the time taken for sliding mode to occur, can be reduced by increasing the corresponding discontinuous control magnitudes. In the time-varying case, the UAV with label three disconnects itself from the swarm and controls its altitude at a value

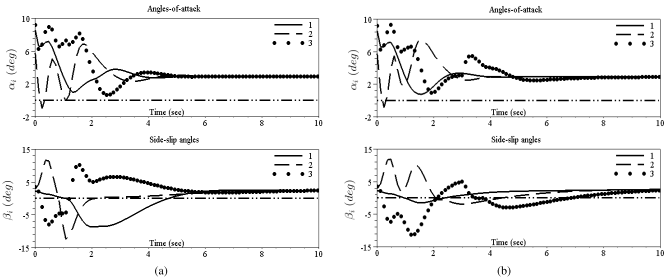

Fig. 4. Control of α and β. (a) Time-invariant topology. (b) Time-varying topology.

of 160 m. The time instant T_C is selected, randomly, as $10/3 = 3.33$ s, where 10 s is the total duration of the simulation. Since the swarm topology changes at $t = T_C$, the switching surfaces of UAV 3 become those designed for the autopilot and hence the values of these functions jump.

The achievement of consensus in the heading angles and the control of the roll angles can be observed in Fig. 3. In the time-varying case, the autopilot of UAV 3 is used to control the heading angle to a value of 150°. The asymptotically decaying behavior of the roll and heading angles, as defined by the switching surfaces, can also be observed in these figures. The errors in control of these states, not presented here, have properties similar to those shown in Fig. 2.

To support the closed-loop analysis presented, the trajectories of α_i and β_i are shown in Fig. 4. As can be observed, in the closed loop, the angles-of-attack achieve a stable positive equilibrium point. In addition, since the UAVs are assumed to fly in the same atmospheric conditions, the UAVs achieve the same values of these states.

A brief discussion on the performance of the proposed controllers when the swarm changes its topology, as per the considered example, is presented. Since for any $t \geq 0$,

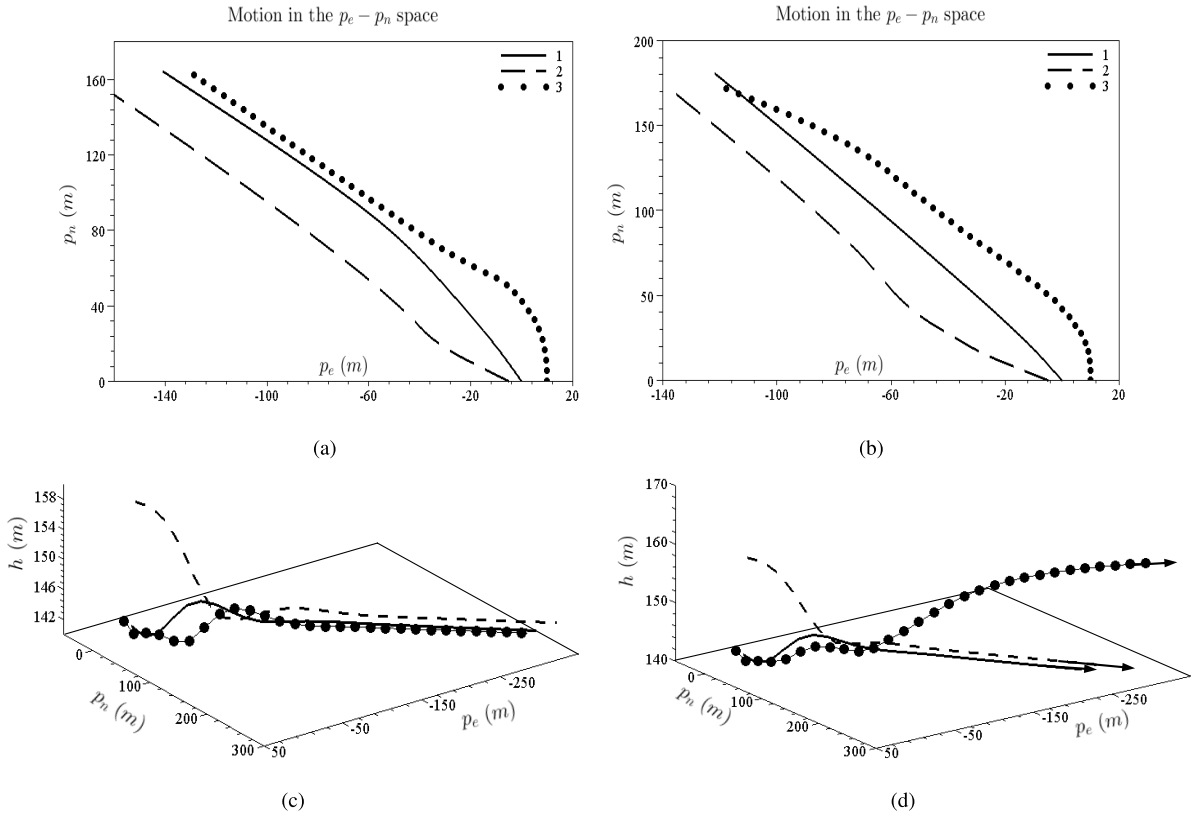

Fig. 5. Locations of the UAVs in the (p_e, p_n) space (a) time-invariant topology and (b) time-varying topology. Locations in the (p_e, p_n, h) space (c) time-invariant topology and (d) time-varying topology.

UAVs 1 and 2 remain connected to each other, intuitively, it is clear that these UAVs will reach a consensus. This result can also be understood by observing that the properties of the Laplacian matrix L_V are the same as that of the original matrix L_I. However, the consensus value will now depend on the time instant when sliding mode occurs on the surfaces defined for these UAVs and when the graph topology changes. For instance, in the current example, from Fig. 2, since sliding mode occurs on $S_{hi} = 0,\ i = 1, 2$ at some time instant, say $t_1 < T_C$, and in addition, since the values of $h_1(t_1), h_2(t_1)$ are the same as those shown in Fig. 2, the final altitude consensus value does not change from the case when the topology is time invariant. Details on the calculation of the consensus value and the time instant when consensus occurs are deferred to a future brief on this topic.

Finally, in Fig. 5, the locations of the UAVs in the (p_e, p_n) and (p_e, p_n, h) spaces are presented. As can be seen, in the time-invariant case, the UAVs fly in the same direction at the same altitude. On the other hand, the location of UAV 3 becomes clearer when it disconnects itself from the swarm. In these figures, the arrows denote the heading angles.

V. Conclusion

With the theoretical and simulation results presented, the proposed algorithms make a connected swarm of UAVs, as well its members, autonomous. Using either the SMC-based autopilot or consensus controllers, the flying characteristics of each UAV become insensitive to disturbances and parameter variations. In terms of future work, the controllers can be designed to provide robustness against gusts of wind and include the property of obstacle avoidance or avoiding other UAVs in the case of dense swarms.

References

[1] W. Ren, "Distributed leaderless consensus algorithms for networked Euler-Lagrange systems," *Int. J. Control*, vol. 82, no. 11, pp. 2137–2149, 2009.

[2] R. W. Beard, T. W. McLain, D. B. Nelson, D. Kingston, and D. Johanson, "Decentralized cooperative aerial surveillance using fixed-wing miniature UAVs," *Proc. IEEE*, vol. 94, no. 7, pp. 1306–1324, Jul. 2006.

[3] O. Ilaya, C. Bil, and M. Evans, "Control design for unmanned aerial vehicle swarming," *Proc. Inst. Mech. Eng., Part G, J. Aerosp. Eng.*, vol. 222, no. 4, pp. 549–567, 2008.

[4] V. Utkin, *Sliding Modes in Control and Optimization*. New York, NY, USA: Springer-Verlag, 1992.

[5] P. P. Menon and C. Edwards, "A discontinuous protocol design for finite-time average consensus," in *Proc. IEEE Int. CCA*, Sep. 2010, pp. 2029–2034.

[6] S. Khoo, L. Xie, and Z. Man, "Robust finite-time consensus tracking algorithm for multirobot systems," *IEEE-ASME Trans. Mech.*, vol. 14, no. 2, pp. 219–228, Mar. 2009.

[7] J. Yao, R. Ordóñez, and V. Gazi, "Swarm tracking using artificial potentials and sliding mode control," in *Proc. 45th IEEE Conf. Decision & Control*, Dec. 2006, pp. 4670–4675.

[8] D. Galzi and Y. Shtessel, "UAV formations control using high order sliding modes," in *Proc. Amer. Control Conf.*, Jun. 2006, pp. 1–5.

[9] S. N. Singh, M. Pachter, P. Chandler, S. Banda, S. Rasmussen, and C. Schumacher, "Input-output invertibility and sliding mode control for close formation flying of multiple UAVs," *Int. J. Robust Nonlinear Control*, vol. 10, no. 10, pp. 779–797, 2000.

[10] G. Campa, Y. Gu, B. Seanor, M. R. Napolitano, L. Pollini, and M. L. Fravolini, "Design and flight-testing of nonlinear formation control laws," *Control Eng. Practice*, vol. 15, no. 9, pp. 1077–1092, 2007.

[11] M. Chiaramonti and G. Mengali, "Control laws for a formation of autonomous flight vehicles," *Aeronautical J.*, vol. 113, no. 1147, pp. 609–616, Sep. 2009.
[12] S. N. Singh, R. Zhang, P. Chandler, and S. Banda, "Decentralized nonlinear robust control of UAVs in close formation," *Int. J. Robust Nonlinear Control*, vol. 13, no. 11, pp. 1057—1078, 2003.
[13] K. Natesan, D.-W. Gu, I. Postlethwaite, and J. Chen, "Design of flight controllers based on simplified LPV model of a UAV," in *Proc. 45th IEEE Conf. Decision & Control*, Dec. 2006, pp. 37–42.
[14] L. H. Carter and J. S. Shamma, "Gain-scheduled bank-to-turn autopilot design using linear parameter varying transformations," *J. Guid., Control, Dyn.*, vol. 19, no. 5, pp. 1056–1063, Sep./Oct. 1996.
[15] C. H. Lee and M. J. Chung, "Gain-scheduled state feedback control design technique for flight vehicles," *IEEE Trans. Aerosp. Electron. Syst.*, vol. 37, no. 1, pp. 173–182, Jan. 2001.
[16] S. K. Spurgeon and R. J. Patton, "Robust variable structure control of model reference systems," *IEE Proc.*, vol. 137, no. 6, pp. 341–348, Nov. 1990.
[17] S. N. Singh, M. Steinberg, and R. D. DiGirolamo, "Variable structure robust flight control system for the F-14," *IEEE Trans. Aerosp. Electron. Syst.*, vol. 33, no. 1, pp. 77–84, Jan. 1997.
[18] E. M. Jafarov and R. Tasaltin, "Robust sliding-mode control for the uncertain MIMO aircraft model F-18," *IEEE Trans. Aerosp. Electron. Syst.*, vol. 36, no. 4, pp. 1127–1141, Oct. 2000.
[19] A. Levant, A. Pridor, R. Gitizadeh, I. Yaesh, and J. Z. Ben-Asher, "Aircraft pitch control via second order sliding technique," *AIAA J. Guid., Control Dyn.*, vol. 23, no. 4, pp. 586–594, 2000.
[20] S. N. Singh, "Asymptotically decoupled discontinuous control of systems and nonlinear aircraft maneuver," *IEEE Trans. Aerosp. Electron. Syst.*, vol. 25, no. 3, pp. 380–391, May 1989.
[21] S. N. Singh, M. Steinberg, and A. B. Page, "Nonlinear adaptive and sliding mode flight path control of F/A-18 model," *IEEE Trans. Aerosp. Electron. Syst.*, vol. 39, no. 4, pp. 1250–1262, Oct. 2003.
[22] T. Keviczky and G. J. Balas, "Receding horizon control of an F-16 aircraft: A comparative study," *Control Eng. Practice*, vol. 14, no. 9, pp. 1023–1033, Sep. 2006.
[23] Y. Kang and J. K. Hedrick, "Linear tracking for a fixed-wing UAV using nonlinear model predictive control," *IEEE Trans. Control Syst. Techonol.*, vol. 17, no. 5, pp. 1202–1210, Sep. 2009.
[24] G. Ducard and H. P. Geering, "Airspeed control for unmanned aerial vehicles: A nonlinear dynamic inversion approach," in *Proc. 16th Medit. Conf. Control Autom.*, Aug. 2008, pp. 676–681.
[25] R. Merris, "Laplacian matrices of graphs: A survey," *Linear Algebra Appl.*, vols. 197–198, no. 1, pp. 143–176, 1994.
[26] R. Olfati-Saber and R. M. Murray, "Consensus problems in networks of agents with switching topology and time-delays," *IEEE Trans. Autom. Control*, vol. 49, no. 9, pp. 1520–1533, Sep. 2004.
[27] S. Rao and D. Ghose, "Sliding mode control-based algorithms for consensus in connected swarms," *Int. J. Control*, vol. 84, no. 9, pp. 1477–1490, 2011.
[28] B. L. Stevens and F. L. Lewis, *Aircraft Control and Simulation*. New York, NY, USA: Wiley, 2003.